#### Research Article

Mehwish Amanat, Tayyaba Shahzadi\*, Tauheeda Riaz, Maria Zaib, Faisal Nawaz, Ahmed M. Tawfeek, Muhammad Ramzan Khawar, Sung Jea Park\*, and Dongwhi Choi\*

# Enhanced catalytic degradation of amoxicillin by phyto-mediated synthesised ZnO NPs and ZnO-rGO hybrid nanocomposite: Assessment of antioxidant activity, adsorption, and thermodynamic analysis

https://doi.org/10.1515/ntrev-2023-0189 received November 12, 2023; accepted December 23, 2023

**Abstract:** Antibiotics are resistant compounds that become emerging contaminants that cause hazards to human health and the ecological environment due to their wide production and consumption. The present research reveals the remediation of amoxicillin (AMX) antibiotic by catalytic degradation using fabricated zinc oxide (ZnO) and zinc oxidereduced graphene oxide (ZnO-rGO) catalysts. The characterization of the catalyst was carried out *via* UV–Vis spectroscopy, Fourier transform infrared spectroscopy, X-ray diffraction, energy dispersive X-ray spectroscopy, and scanning electron

microscopy to evaluate the morphology and composition of synthesised catalyst. The catalytic ability of ZnO-rGO and ZnO was investigated by analysing the degradation of AMX. The ZnO-rGO nanocomposites (NCs) showed improved catalytic performance towards AMX degradation (96%) than pure ZnO nanoparticles (85%), which may be attributed to the incorporation of rGO, which enhanced the adsorption rate and changed the electron-hole recombination rate. The antioxidant potential of synthesised nanomaterials was also analysed by three different methods. The adsorption behaviour was explained through the Langmuir and Freundlich models, and the results revealed that AMX adsorption followed the Freundlich model more closely for both catalysts. The adsorption of AMX was also studied thermodynamically at different temperatures. The negative Gibbs energy change, positive enthalpy change, and entropy change showed the reaction's spontaneity and endothermic nature. Finally, it can be assumed that the ZnO-rGO NCs could be an effective semiconductor for the degradation of AMX from wastewater.

**Keywords:** ZnO-rGO nanocomposite, *Litchi chinensis*, amoxicillin, adsorption, catalytic removal

**Faisal Nawaz:** Department of Basic Sciences, University of Engineering and Technology Lahore, Faisalabad, Pakistan

**Ahmed M. Tawfeek:** Department of Chemistry, College of Science, King Saud University, Riyadh 11451, Saudi Arabia

**Muhammad Ramzan Khawar:** Department of Mechanical Engineering (Integrated Engineering Program), Kyung Hee University, 1732 Deogyeong-daero, Yongin, Gyeonggi, 17104, Republic of Korea

## 1 Introduction

The entry of different emerging pollutants into water bodies has now become a major environmental threat. In recent years, pharmaceutical products specifically antibiotics have been identified as the most common contaminants found in various water sources, including drinking water, groundwater, and surface water. Various sources such as domestic sewage, human and animal excretion, pharmaceutical manufacturing plants, hospital effluents, and agriculture release pharmaceutical compounds into

<sup>\*</sup> Corresponding author: Tayyaba Shahzadi, Department of Chemistry, Government College for Women University Sialkot, Sialkot, Pakistan, e-mail: tayyaba332@gmail.com

<sup>\*</sup> Corresponding author: Sung Jea Park, School of Mechanical Engineering, Korea University of Technology and Education, 1600 Chungjeol-ro, Cheonan, Chungnam, 31253, Republic of Korea; Future Convergence Engineering, Korea University of Technology and Education, 1600 Chungjeol-ro, Cheonan, Chungnam, 31253, Republic of Korea

<sup>\*</sup> Corresponding author: Dongwhi Choi, Department of Mechanical Engineering (Integrated Engineering Program), Kyung Hee University, 1732 Deogyeong-daero, Yongin, Gyeonggi, 17104, Republic of Korea Mehwish Amanat, Tauheeda Riaz: Department of Chemistry, Government College for Women University Sialkot, Sialkot, Pakistan Maria Zaib: Department of Chemistry, University of Jhang, Sialkot, Pakistan

the water [1]. The antibiotics that enter water bodies and the soil ecosystem cause endocrine disruption and the emergence of antibiotic resistance in microorganisms [2]. In microorganisms, resistance to  $\beta$ -lactams is caused by chromosomal mutations in cell-wall-synthesizing enzymes known as penicillin-binding proteins (PBPs). Such mutations in PBPs are caused by a continuous mutation process that causes resistance [3]. So, it is important to remove and degrade antibiotics from aqueous media to protect the ecosystem.

Amoxicillin (AMX) is a semisynthetic beta-lactam antibiotic that belongs to the penicillin family and destroys bacterial cell walls. It is used to cure human as well as animal infectious diseases caused by susceptible microorganisms. It is the most widely used antibiotic in the penicillin family because of its ability to be absorbed orally. However, unfortunately, AMX is hardly degradable [4].

In the literature, various treatment techniques have been utilized to eliminate antibiotics from an aqueous medium, such as biodegradation [5], flocculation [6], membrane filtration [7], adsorption [8], and various advanced oxidation processes such as ozonation [9] and semiconductor photocatalysis [10]. Among all these approaches, the adsorption process is one of the most potent techniques used to remove organic contaminants from aqueous media owing to its high removal capacity, simplicity, and low operation cost [11].

Different adsorbent materials, *i.e.*, reduced graphene oxide (rGO), carbon nanotubes, activated carbon, magnetic graphene oxide, metal/metal oxide nanoparticles (NPs), and graphene-based nanocomposites (NCs), have been used for antibiotics removal methods [8].

Zinc oxide (ZnO) NPs were chosen as they possess remarkable properties such as a large specific surface area, nano size, broad bandgap (3.37 eV), chemical and physical inertness, non-toxicity, high adsorption capacity, easy to synthesize, biocompatibility, excellent electronic, catalytic, and optical properties [12]. Various approaches have been applied to increase the effectiveness of ZnO NPs. One of the most favourable strategies is the coupling of ZnO NPs with graphene and its derivatives to enhance catalytic performance by enlarging surface area and suppressing electron—hole recombination rates in ZnO [13]. Many antibiotics such as beta-lactams have aromatic rings in their structure, which make the graphene-based material an excellent adsorbent for the removal of antibiotics  $via \pi - \pi$  interactions [14].

Green synthesis provides significant advantages over traditional approaches and a wide range of biological applications. It avoids the use of toxic reagents and the production of undesirable by-products by offering sustainable synthesis methods. The use of plant leaf extract in the synthesis of metal NPs is one of the most compatible, safe, and environmentally friendly methods.

Plant extracts contain a variety of bioactive compounds, including alkaloids, flavonoids, and phenols, which help to stabilise and control the size of NPs [15].

Phyto-mediated synthesised ZnO NPs exhibited many biomedical applications such as antibacterial, anti-inflammatory, and antioxidant. ZnO NPs have received a lot of interest due to their antioxidant properties, which are significant in resisting oxidative stress in biological systems. ZnO NPs have the potential to scavenge reactive free radicals produced by oxidative stress, which cause a variety of diseases such as cancer and neurological diseases. As antioxidants, ZnO NPs neutralise free radicals and minimise oxidative damage. ZnO NPs as antioxidants neutralize free radicals and reduce oxidative damage [16].

The present work reports the green synthesis of ZnO NPs and ZnO-rGO NCs by using an aqueous leaf extract of the *Litchi chinensis* plant as a reducing and capping agent for the first time. The properties of prepared nanomaterials were analysed by different characterization techniques, and the efficiency of synthesised nanomaterials in AMX degradation was also assessed.

## 2 Materials and methods

#### 2.1 Chemicals

Leaves of L. chinensis were taken from the local area of Sialkot. The analytical grade chemical reagents used in this study were graphite powder,  $Zn(NO_3)_2\cdot 6H_2O$ ,  $KMnO_4$ ,  $H_2O_2$ ,  $H_2SO_4$ , DPPH radical (1,1-diphenyl-2-picrylhydrazyl), methanol, Folin–Ciocalteu reagent,  $Na_2CO_3$ , ammonium hexamolybdate,  $Na_3PO_4$ , NaOH, and HCl.

## 2.2 Preparation of plant leaf extract

Plant leaves were thoroughly washed with distilled  $\rm H_2O$ , dried under shade, and crushed. For preparing aqueous plant extract, 2 g of powdered leaves were added to 100 mL of distilled water and heated at 80°C for 60 min. The extract was filtered and then placed at 5°C for further use [17].

#### 2.3 Preparation of ZnO NPs

A solution of 2.97 g (1 M) of Zn(NO<sub>3</sub>)<sub>2</sub>·6H<sub>2</sub>O in 10 mL of DW was prepared. Afterwards, 10 mL of plant extract was mixed with a salt solution in a 1:1 ratio and stirred for 60

min at 60°C using a magnetic stirrer. The transformation of colour from yellow to brown indicates the formation of NPs. After centrifugation, NPs were washed with distilled H<sub>2</sub>O to obtain pure ZnO NPs [18].

## 2.4 Preparation of graphene oxide and ZnOrGO NC

Graphene oxide was prepared *via* the modified Hummers method [34]. To synthesize ZnO-rGO NCs, 0.1 g graphene oxide was transferred into distilled H<sub>2</sub>O (20 mL) and sonicated for 60 min to get a homogeneous mixture. Then, 20 mL solution of 2.97 g Zn(NO<sub>3</sub>)<sub>2</sub>·6H<sub>2</sub>O was mixed with rGO dispersion and stirred for 60 min. Then, 40 mL of plant extract was slowly poured into the resulting mixture and then centrifuged. The solid residues were dried overnight at 60°C to get ZnO-rGO NCs [17].

## 2.5 Determination of point zero charge (pHpzc)

To determine the pHpzc of both synthesised ZnO NPs and ZnO-rGO, 40 mL of 0.1 M NaCl solution was taken in different beakers, and the initial pH (pHi) from 2 to 12 was adjusted using 0.1 M HCl and NaOH solutions. After maintaining pHi, the desired amount of synthesised nanomaterials was added to all beakers and stirred at the speed of 150 rpm on an orbital shaker at room temperature for 24 h. After that, the final pH was measured. The pHpzc was calculated by plotting the graph between pHi and ΔpH [19].

#### 2.6 Characterization

The formation of prepared nanomaterials was confirmed using a UV-Vis spectrophotometer (Specord 210 plus, Analytic Jena AG, Germany), Fourier transform infrared (FTIR), scanning electron microscopy (SEM), energy-dispersive X-ray (EDX) spectroscopy (JEOL JAPAN), and X-ray diffraction (XRD, X-PERT PANalytical diffractometer). High-performance liquid chromatography (HPLC) analysis was performed to analyse the degradation of AMX with Waters Alliance™ e2695 XE HPLC instrument.

## 2.7 Antioxidant potential

Antioxidant potential of green synthesised nanomaterials was determined by three different methods.

#### 2.7.1 DPPH free radical scavenging activity

DPPH radical scavenging capacity of prepared ZnO NPs and ZnO-rGO was determined by the standard method [20]. To determine free radical scavenging ability, different concentrations (500, 1,000, and 1,500 µg/mL) of synthesised nanomaterials were taken. Then, 3 mL of DPPH solution, which was prepared by adding 4 mg of DPPH in 100 mL of methanol, was added and shaken vigorously. The mixture was kept for 30 min at room temperature in the dark and centrifuged for 10 min at 3,000 rpm. The colour of the solution changed from violet to yellow, indicating that the DPPH radical was reduced. The absorbance of the supernatant was recorded using a spectrophotometer at 517 nm. The DPPH radical scavenging capacity of synthesised nanomaterials was calculated using this formula:

%Scavenging activity
$$= \frac{\text{Control absorbance} - \text{Sample absorbance}}{\text{Control absorbance}} \times 100.$$
(1)

#### 2.7.2 Total phenolic contents (TPCs)

The TPCs were measured by the method of Makkar et al. using the Folin-Ciocalteu reagent [21]. The TPC was determined by adding 0.5 mg/mL of prepared nanomaterials in 0.1 mL Folin-Ciocalteu reagent (2 N). Then, 2.8 mL of 10% Na<sub>2</sub>CO<sub>3</sub> was added to the mixture and shaken vigorously. The solution was stored at room temperature for 40 min, and then absorbance was recorded at 765 nm. TPC was calculated as mg of gallic acid equivalents per gram of sample by extrapolation of different concentrations of gallic acid.

#### 2.7.3 Total antioxidant activity

The total antioxidant capacity was measured by the phosphomolybdate method [22]. About 0.5 mg/mL of synthesised nanomaterials were mixed with 4 mL of reagent solution (4 mM of ammonium molybdate, 28 mM of sodium phosphate, and 0.6 mM of sulphuric acid). The mixture was taken in test tubes, which were then sealed and heated in the water bath at 95°C for 90 min, and then the solution was cooled. After cooling, the absorbance of the solution was checked at 695 nm. The typical blank solution consisted of 4 mL of reagent solution and was heated under the same conditions as the sample solution.

## 2.8 Adsorption studies

The batch experiment was performed to compare AMX removal by ZnO and ZnO-rGO with 5 mg/L of AMX solution. The appropriate amount of catalyst was mixed into 25 mL of AMX solution, placed in a shaker for 60 min, and then centrifuged. The absorbance value of the supernatant after centrifugation was determined, and the equilibrium concentration  $C_{\rm e}$  (mg/L) was converted from the standard concentration curve of AMX. The adsorption capacity is measured using the following formula [23]:

$$q_{\rm e} = \frac{C_0 - C_{\rm e}}{M} \times V, \tag{2}$$

where initial and equilibrium concentrations of AMX are  $C_0$  and  $C_e$  (mg/L), respectively, V is the volume of the AMX solution (L), and M (g) is the adsorbent quantity.

The AMX degradation efficiency is calculated by using the following equation [24]:

%Degradation efficency = 
$$\frac{C_i - C_f}{C_i} \times 100$$
. (3)

## 3 Results and discussion

# 3.1 Proposed mechanism for the formation of ZnO NPs

In the green preparation of ZnO NPs, potential phytochemical agents present in the leaves of L. chinensis plant, such as polyphenols (epicatechin), reduced  $Zn^{2+}$  to ZnO or aggregates of ZnO NPs, as shown in Figure 1a; first, zinc nitrate hexahydrate was ionized in aqueous media to give  $Zn^{2+}$ 

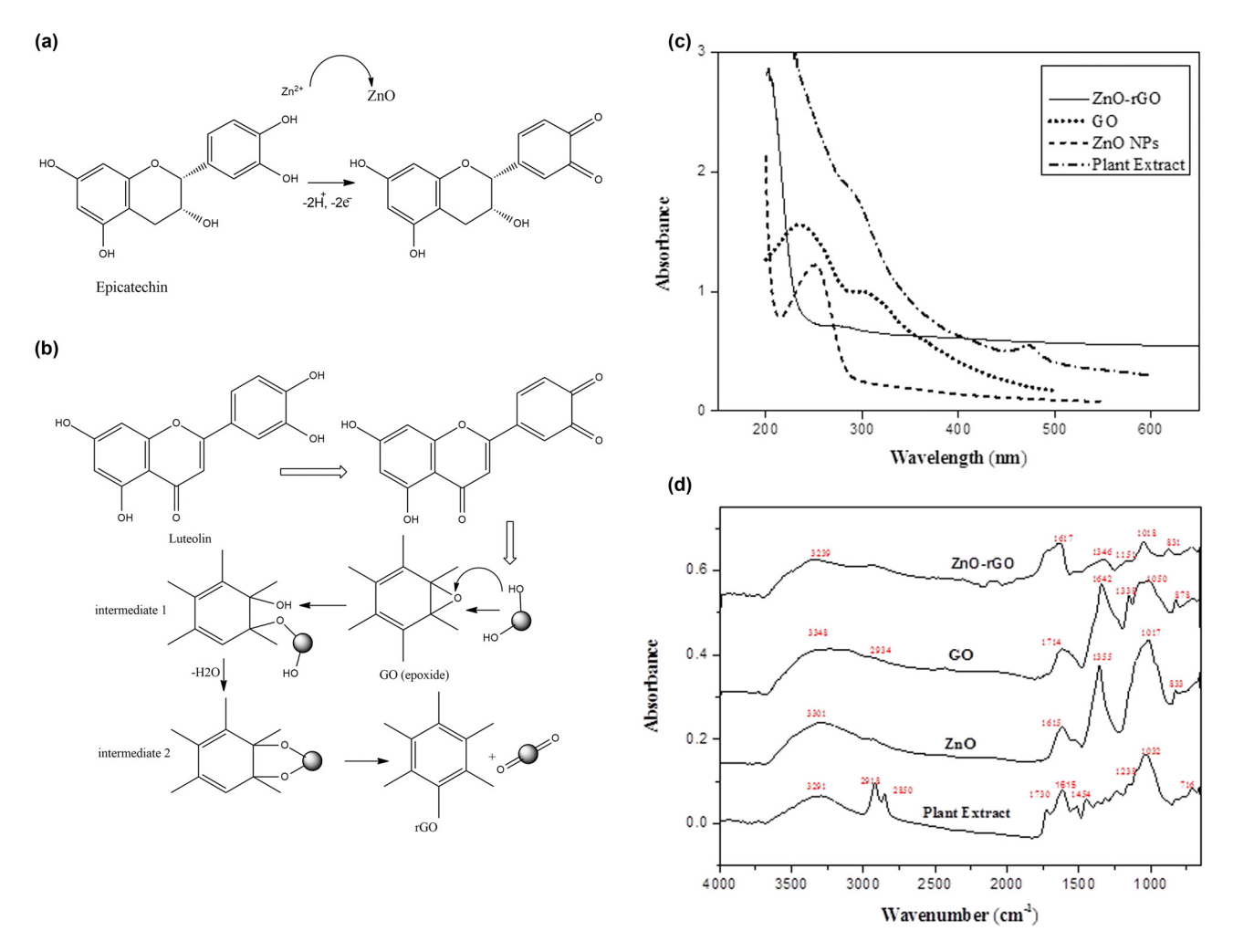


Figure 1: (a) Proposed mechanism for synthesis of ZnO NPs; (b) proposed mechanism for the reduction of GO to rGO; (c) UV–Vis spectra of plant extract, ZnO, GO, and ZnO-rGO; and (d) FTIR spectra of plant extract, ZnO, GO, and ZnO-rGO.

ions which reacted with epicatechin and formed Zn-epicatechin. It oxidized to quinone and produced electrons and hydrogens, which reduced Zn<sup>2+</sup> ions into ZnO NPs [25].

# 3.2 Proposed mechanism for reduction of GO to rGO by plant extract

The reducing agents (polyphenols) in the leaf extract of the L. chinensis plant reacted with graphene oxide, as depicted in Figure 1b. The epoxide group of GO came into contact with the alcohol group. The epoxide and phenolic groups of GO generated an intermediate due to the nucleophilic attack of the -OH groups, and the water was removed. After reduction, rGO was produced [26].

### 3.3 Characterization of ZnO NCs

The absorption spectra of plant extract, ZnO NPs, GO, and ZnO-rGO NCs are shown in Figure 1c. The spectrum of ZnO NPs displayed a single broad and strong peak at 250 nm because of surface plasmon resonance. GO absorption peaks in aqueous suspension were detected at 234 nm and a weak peak at 305 nm. The peak at 234 nm was caused by  $\pi \to \pi^*$  transition of aromatic -C=C bonds, and the small peak observed at 305 nm was caused by  $n\to\pi^*$  transition of -C=O bonds of carboxyl and carbonyl groups. The ZnO-rGO absorption spectrum showed a broad peak in the 250–300 nm range. Compared to the GO absorption spectrum, the peak at 234 nm was shifted to 274 nm after reduction, and a weak peak at 305 nm vanished completely due to carboxylic acid group reduction with the regeneration of graphitic nature in ZnO-rGO NCs [27,28]. As a result of

the above-mentioned observations, the position of the NC absorption peaks was very close to individual peaks, indicating a strong reaction between ZnO NPs and rGO in ZnO-rGO NCs.

The FTIR spectra of plant leaf extract, ZnO, GO, and ZnO-rGO are presented in Figure 1d. The FTIR spectrum of L. chinensis leaf extract showed a broad peak at 3,229 cm<sup>-1</sup> assigned to vibrational stretching of -OH groups that arise due to the presence of phenols, carbohydrates, and alcohols. The peaks at 2,918 and 2,850 cm<sup>-1</sup> regions correspond to C-H stretching of CH<sub>3</sub> and CH<sub>2</sub> functional groups of alkanes, and a band at 1,730 cm<sup>-1</sup> was ascribed to -C=0 stretching vibration of aldehyde, ketone, carboxylic acid, and ester. The vibrational peaks at 1,615, 1,515, and 1,454 cm<sup>-1</sup> were also noted, which were ascribed to the bending of N-H bonds originating from amines or amides and aromatic C=C stretching. The peaks at 1,371 and 1,238 cm<sup>-1</sup> originated from the bending of the -OH group of phenol and C-O or C-N stretching, respectively, while the corresponding peaks at 1,032 and 716 cm<sup>-1</sup> were attributed to the C-O stretch of esters or ethers and C-X stretching [25].

When the spectra of ZnO NPs were compared with the spectra of *L. chinensis* leaf extract, shifting of peaks was observed in spectra, indicating the reduction of molecules. As a result, secondary metabolites, such as polyphenol functional groups, covered the ZnO NPs. From FTIR analysis, it was confirmed that bioactive compounds present in plant leaves performed dual functions for the synthesis and stabilization of ZnO NPs [29].

FTIR spectra of graphene oxide showed various characteristic absorption peaks (Figure 1d). A broad absorption peak that appeared at 3,348 cm<sup>-1</sup> indicated –OH groups stretching vibrations present on graphene sheets and water absorbed on the surface of GO. The typical absorption peak at 2,934 cm<sup>-1</sup> was assigned to CH<sub>2</sub> stretching, and the peak at 1,714 cm<sup>-1</sup> represented the –C=O stretching of carboxyl

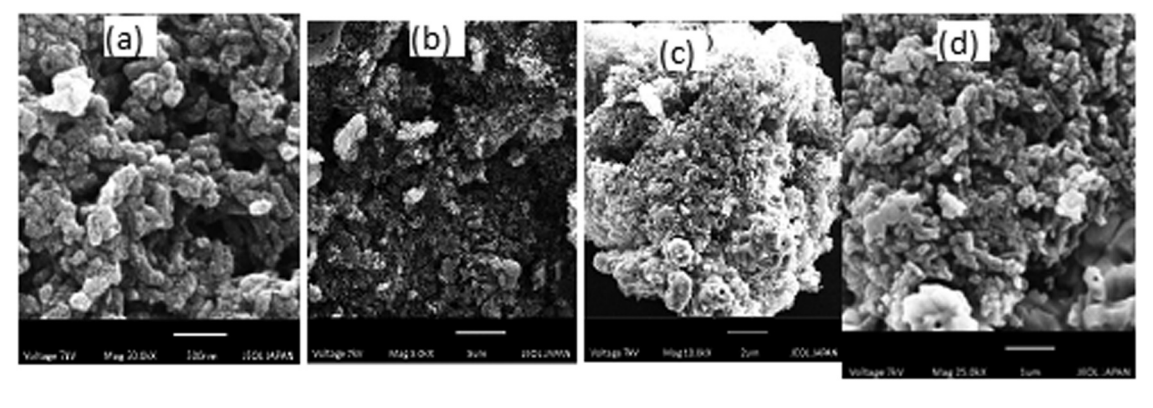


Figure 2: SEM images of ZnO NPs: (a) 500 nm, (b) 5  $\mu$ m, (c) 2  $\mu$ m, and (d) 1  $\mu$ m.

groups. Absorption peaks at 2,088 and 1,642 cm $^{-1}$  were attributed to -N=C=O and -C=C stretch. Peaks observed at 1,338, 1,050, and 878 cm $^{-1}$  were ascribed to stretching peaks of C-O epoxy and alkoxy groups and bending vibration =C-H. The presence of functional groups containing oxygen proved that the graphite was oxidized to GO, and the occurrence of hydroxyl groups allowed GO to quickly establish hydrogen bonds with  $H_2O$ , giving it a hydrophilic appearance [30,31].

The FTIR spectrum of ZnO-rGO NCs displayed various representative absorption bands. Compared with GO spectra, the intensity of the –OH peak at 3,239 cm<sup>-1</sup> in ZnO-rGO NCs reduced dramatically due to the loss of –OH groups, which might be due to the bonding of –OH groups with ZnO NPs, while the absorption peak at 1,714 cm<sup>-1</sup> for C=O was absent in NCs compared to GO, confirming the GO reduction. The stretching peak at 1,151 cm<sup>-1</sup> represented a more powerful Zn–O–C combination. It is worth noting that after reduction, peaks of GO either vanished or appeared with considerably reduced intensities. These results are consistent with the literature [32].

SEM analysis was conducted to analyse the morphology of nanomaterials. The SEM images of ZnO NPs have distinct spherical and hexagonal morphologies (Figure 2). The ZnO NPs that were synthesised were random [33]. The ZnO-rGO NCs were made up of clumps of ZnO nanostructures that were well anchored on the rGO sheet (Figure 3).

The EDX analysis was carried out to evaluate the chemical composition of prepared samples. The EDX spectra in Figure 4a and b showed the elemental composition of ZnO NPs and ZnO-rGO NCs. It revealed that all the predictable elements were available in the prepared nanomaterials. It also showed the high-purity composition of the samples by detecting only the peaks of elements in NCs. The peaks shown in the ZnO-rGO spectrum were attributed to zinc, oxygen, and carbon constituents. No other peaks of impurities were detected in the spectra [34].

XRD patterns of ZnO NPs and ZnO-rGO are shown in Figure 4c. The strong prominent peaks on  $2\theta$  values of 31.7°,

34.4°, 36.2°, 47.5°, 56.6°, 62.8°, 66.4°, and 67.9°, for ZnO NPs, and 31.7°, 34.4°, 36.2°, 47.5°, 56.6°, 62.8°, 67.9°, 69.1°, 72.6°, and 76.9°, for NCs were observed. XRD spectra of ZnO NPs exhibited a series of diffraction peaks that perfectly indexed to highly crystalline, spherical, and hexagonal wurtzite structural patterns of ZnO NPs from JCPDS card No. 46-145. When compared to ZnO NPs, XRD spectra of prepared ZnO-rGO NCs exhibited no significant difference in peak shapes and locations, showing that the addition of rGO had no effect on the orientations of crystals of ZnO NPs. There were no peaks identified that could be attributed to foreign impurities. An average crystallite size of the ZnO NPs and ZnO-rGO NCs were 23.4 and 18.7 nm, which were calculated by the Debye–Scherrer equation [35]:

$$D = \frac{k\lambda}{\beta\cos\theta}.$$

## 3.4 Adsorption studies

#### 3.4.1 Adsorbent dosage effect

Adsorbent dosage effects of ZnO NPs and ZnO-rGO NCs on degradation efficiency of AMX were studied in the range of 0.5-10 mg by keeping AMX solution concentration constant (5 mg/L, V=25 mL) for 1. The degradation efficiency decreased by increasing the dosage, as shown in Figure 5(a). This might be attributed to decreased light penetration, increased light scattering, and aggregation of ZnO-rGO NCs in aqueous solution at high adsorbent amounts, which greatly reduced the surface area for adsorption. In the case of ZnO NPs, initially, the degradation efficiency increased by increasing the catalyst amount owing to more binding sites and then declined due to the agglomeration of particles [36]. The result indicated that the degradation efficiency of ZnO-rGO NCs (96% at 0.5 mg) was maximum as compared to ZnO NPs (88% at 5 mg).

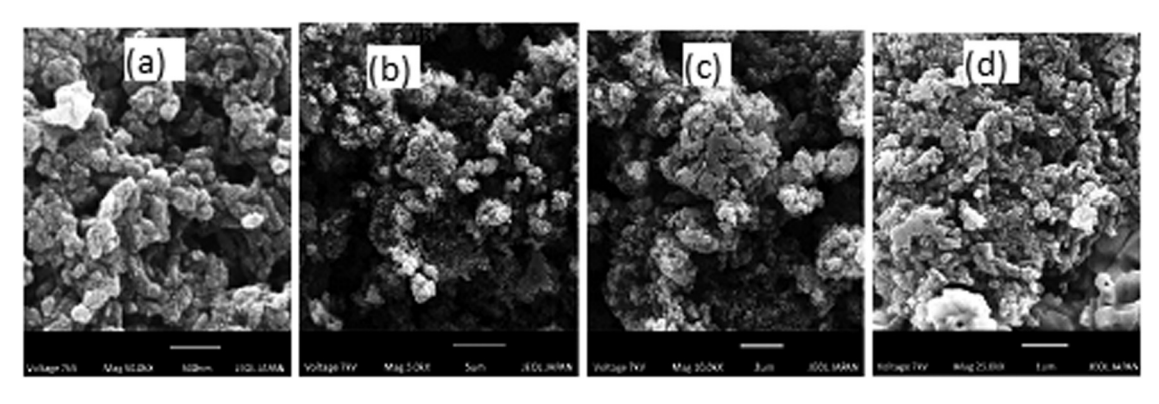


Figure 3: SEM images of ZnO-rGO NCs: (a) 500 nm, (b) 5  $\mu$ m, (c) 2  $\mu$ m, and (d) 1  $\mu$ m.

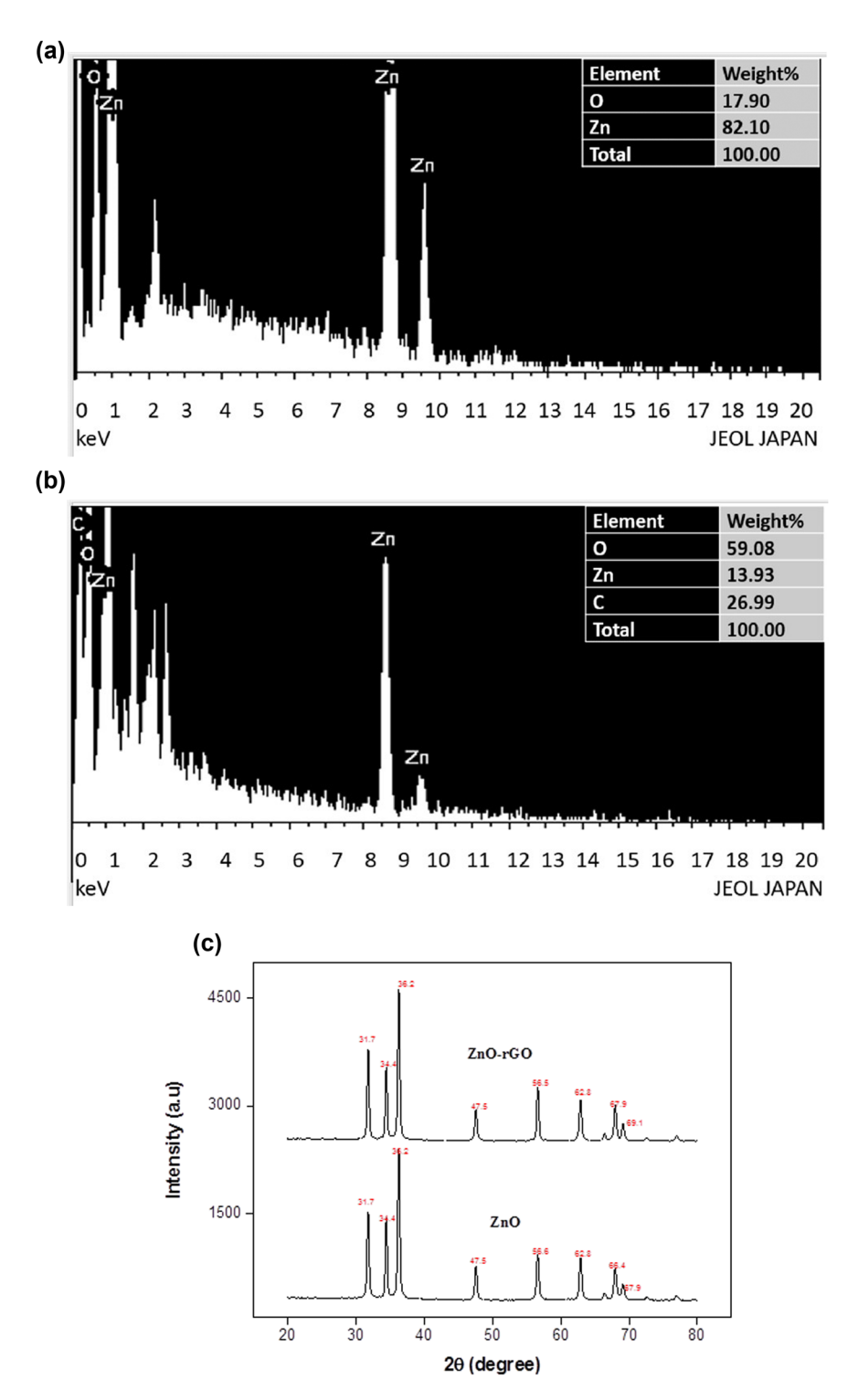


Figure 4: (a) EDX spectrum of ZnO NPs, (b) EDX spectrum of ZnO-rGO NCs, and (c) XRD spectra of ZnO and ZnO-rGO.

#### 3.4.2 Effect of initial AMX concentration

The influence of AMX initial concentration was studied by adjusting AMX solution concentration from 5 to 25 mg/L (V = 25 mL) and keeping the amounts of both catalysts

constant (ZnO = 5 mg, ZnO-rGO = 0.5 mg) for a contact time of 60 min. The results are presented in Figure 5(b), which revealed that at a lower concentration (5 mg/L), maximum degradation of AMX occurred as compared to higher concentrations because active sites present on

catalysts were sufficient, whereas, at a higher concentration, degradation of AMX dropped because more and more molecules of AMX adsorbed on the catalyst's surface and fully covered the surface of active sites and also reduced the generation of active oxidizing 'OH radicals which decreased the degradation of AMX. The saturated active sites of catalysts showed repulsion for incoming AMX molecules and reduced adsorption [37]. The result showed that ZnO-rGO has greater degradation efficiency (92%) compared to ZnO NPs (83%) at the same AMX concentration and reaction time.

#### 3.4.3 Effect of pH

To find out the effect of pH on AMX degradation, the pH was adjusted from 2 to 10 by keeping the concentration of AMX solution and catalysts constant during the entire experiment. The pH of the original AMX solution was 6. The result is presented in Figure 5(c), which depicts that the degradation of AMX increased by increasing the pH of the solution. The highest degradation of AMX occurred in an alkaline medium could be due to two facts. First, the presence of a large number of  $OH^-$  ions on the surface and in an aqueous solution promoted 'OH radical formation that has been regarded as potent oxidizing agents in catalytic processes that initiate degradation of adsorbed AMX molecules. Second, the reason was hydrolysis of AMX attributed to  $\beta$ -lactam ring's instability at high pH [38].

#### 3.4.4 Temperature effect

The temperature effect on AMX degradation efficiency was evaluated at four temperatures (308, 318, 328, and 338 K). The percentage degradation increased by increasing the temperature as presented in Figure 5(d). This might be attributed to the presence of more adsorbent sites because of the activation of adsorbent surfaces at high temperatures. The rate of diffusion of AMX molecules from aqueous solution onto the adsorbent surface enhanced as the temperature elevated. The removal of AMX was facilitated at higher temperatures due to the breakdown of the C–N bond of the β-lactam ring [39]. The result illustrated that AMX adsorption on the adsorbent's surface was endothermic.

#### 3.4.5 pHpzc of ZnO and ZnO-rGO

The pHpzc values calculated for synthesised nanomaterials were 5.2 (ZnO Nps) and 5.4 (ZnO-rGO), as shown in Figure 5(e).

The pHpzc is the value of pH at which the adsorbent surface is neutral. When the solution's pH is less than pHpzc, the adsorbent surface has a positive charge and vice versa. In this case, the pH of the solution is 6, which is higher than pHpzc. As a result, the synthesised adsorbents are negatively charged [40].

### 3.5 Antioxidant potential

#### 3.5.1 DPPH free radical scavenging activity

The free radical scavenging activity of nanomaterials was evaluated by DPPH (1,1-diphenyl-2-picrylhydrazyl), a stable free radical organic molecule. The DPPH scavenging method based on DPPH molecule reduction. The antioxidant activity of synthesised nanomaterials is owing to their reducing power. Nanomaterials neutralized DPPH free radicals and formed a yellow-coloured stable non-radical molecule. The disappearance of the purple colour indicated the scavenging potential of nanomaterials [41]. The results presented in Figure 6 showed that with the increase in the amount of prepared nanomaterials, the ability to scavenge DPPH free radicals also increased. The scavenging ability of ZnO-rGO (93%) was greater than that of ZnO NPs (88%). It was observed that ZnO-rGO composites were effective in inhibiting DPPH, which was primarily caused by electron charge transfer.

#### 3.5.2 TPCs

Using Folin–Ciocalteu reagents, the TPCs of ZnO and ZnO-rGO synthesised by the *L. chinensis* plant were determined spectrophotometrically. This method relies on the formation of the blue complex as a result of the interaction of phenolic compounds with the Folin–Ciocalteu reagent [42]. The calculated TPC of nanomaterials was measured as given in Table 1. The result implied that ZnO-rGO showed a high TPC, *i.e.*, 71.6  $\pm$  0.02 mg/g GAE compared to ZnO 45.7  $\pm$  0.04 mg/g GAE.

#### 3.5.3 Total antioxidant activity

The total antioxidant capacity of synthesised nanomaterials was assessed spectrophotometrically using the phosphomolybdenum method. This method depends on the reduction of Mo(vi) to Mo(v) by antioxidants contained in the sample material at an acidic pH, which results in the

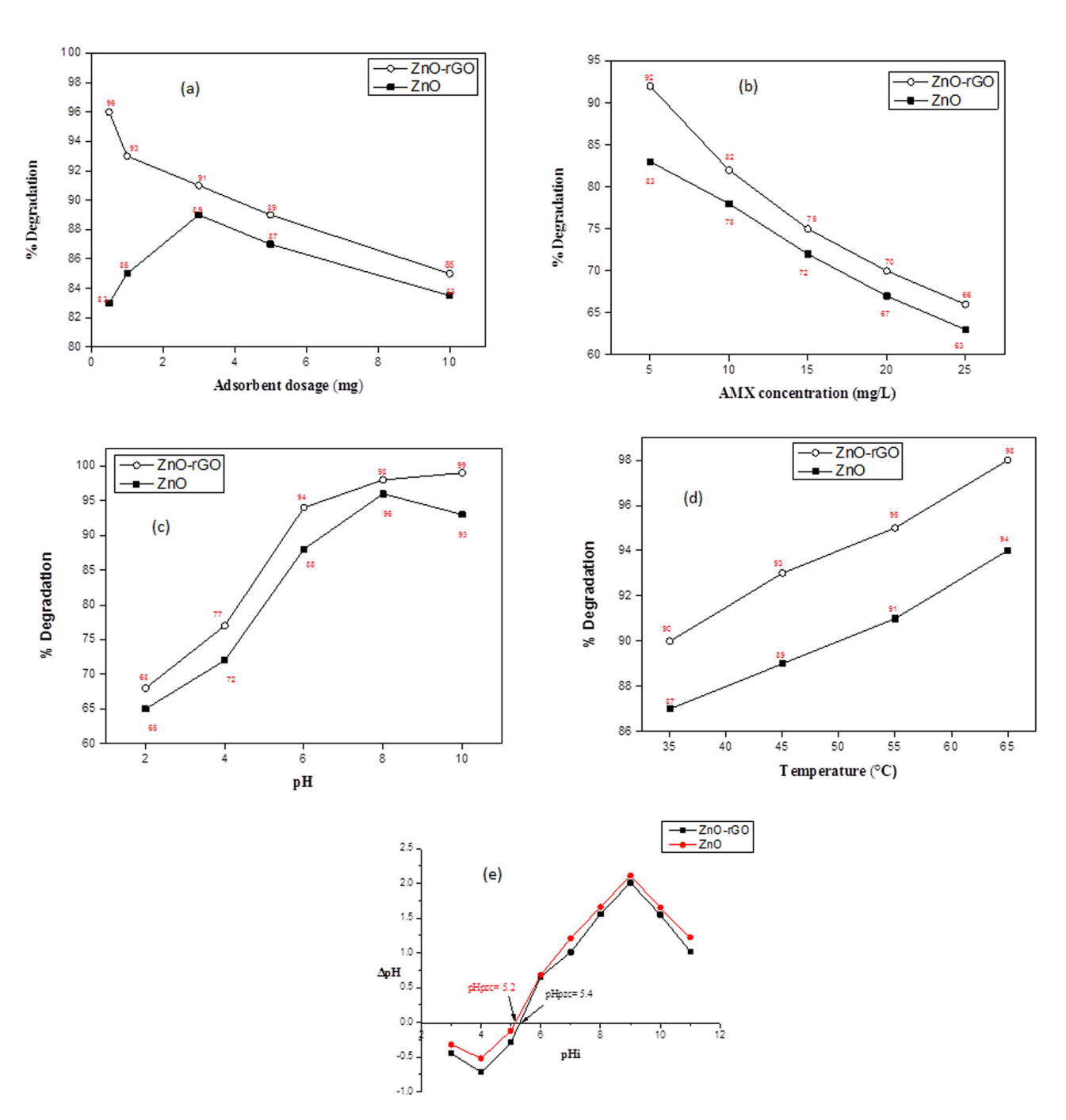


Figure 5: (a) Effect of adsorbent amount on AMX degradation efficiency, (b) influence of initial AMX concentration on its degradation efficiency, (c) pH effect on the AMX degradation efficiency, (d) effect of temperature on degradation efficiency of AMX, and (e) determination of pHpcz of ZnO and ZnO-rGO.

preparation of the green-coloured phosphate-molybdenum complex, commonly used to identify the antioxidants such as phenolic, carotenoids, and tocopherols [41]. The results of total antioxidant activity are presented in Table 1, which indicates that the antioxidant activity of prepared ZnO-rGO (0.644  $\pm$  0.04) was better than that of ZnO NPs (0.510  $\pm$  0.01).

**DE GRUYTER** 

## 3.6 Adsorption isotherm

The adsorption isotherm is the most essential parameter that summarises how adsorbate molecules interact with the adsorbent. This study used the two most common isotherm models, Langmuir and Freundlich. A linear form of

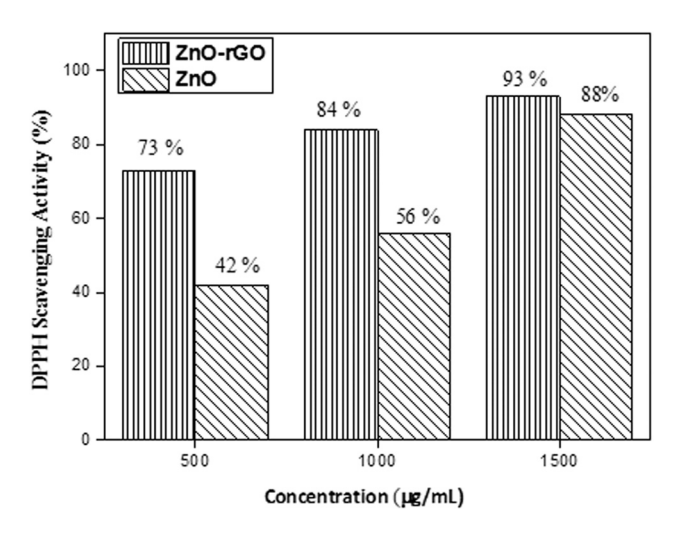


Figure 6: % Scavenging of DPPH radical by ZnO NPs and ZnO-rGO NCs.

Table 1: Results of total phenolic content and total antioxidant activity

Sample	TPC (GAE mg/g of sample)	Total antioxidant activity
ZnO NPs	45.7 ± 0.04	0.510 ± 0.01
ZnO-rGO NCs	71.6 ± 0.02	$0.644 \pm 0.04$
Blank	11.2 ± 0.03	_
BHT		0.813 ± 0.05

Langmuir and Freundlich isotherm models is presented by the following equations [43]:

$$\frac{c_{\rm e}}{q_{\rm e}} = \frac{c_{\rm e}}{q_{\rm m}} + \frac{1}{K_{\rm L} \cdot q_{\rm m}},\tag{4}$$

$$\log q_{\rm e} = \log K_{\rm f} + \frac{1}{n} \log c_{\rm e},\tag{5}$$

where  $q_{\rm e}$  is the amount of AMX adsorbed at equilibrium,  $C_{\rm e}$  is the equilibrium concentration of AMX in solution,  $q_{\rm m}$  is maximum adsorption capacity, and  $K_{\rm L}$  is the Langmuir constant. The values of  $q_{\rm m}$  and  $K_{\rm L}$  were obtained from the plot  $C_{\rm e}/q_{\rm e}$  vs  $C_{\rm e}$ , and the values of  $K_{\rm f}$  and 1/n were derived from the plot of  $\log q_{\rm e}$  vs  $\log C_{\rm e}$ .

The isotherm parameters are shown in Table 2, indicating the value of  $\mathbb{R}^2$  (correlation coefficient) for both

Table 2: Langmuir and Freundlich isotherm parameters

		Langmuir		Fı	reundlich	า
Adsorbent	q <sub>m</sub> (mg/g)	K <sub>L</sub> (L/mg)	R <sup>2</sup>	K <sub>f</sub> (mg/g)	1/n	R <sup>2</sup>
ZnO	109.7	0.25	0.988	23.7	0.554	0.991
ZnO-rGO	909.0	0.53	0.928	328.3	0.395	0.981

models was >0.9, but AMX adsorption on ZnO and ZnO-rGO was better explained by the Freundlich model because the values of  $\mathbb{R}^2$  for Freundlich were greater than  $\mathbb{R}^2$  for the Langmuir model. A similar result was reported in the literature [44]. The 1/n value described the favourability if its value was less than 1, it indicated that adsorption was favourable [45].

## 3.7 Thermodynamics studies

Thermodynamic parameters for the adsorption of AMX on ZnO NPs and ZnO-rGO NCs were examined at four different temperatures (308, 318, 328, and 338 K). It was demonstrated that higher temperatures enhanced AMX adsorption on both adsorbents. Thermodynamic parameters including  $\Delta G^0$ ,  $\Delta H^0$ , and  $\Delta S^0$  are calculated using the following equations:

$$\Delta G = -RT \ln K_{\rm d}. \tag{6}$$

$$K_{\rm d} = \frac{q_{\rm e}}{C_{\rm e}},\tag{7}$$

$$\ln K_{\rm d} = \frac{\Delta S^0}{R} - \frac{\Delta H^0}{RT},\tag{8}$$

where  $K_{\rm d}$  depicts the distribution coefficient, R is the general gas constant (8.314 J/mol K), and T is the temperature (K).

Thermodynamic parameters are presented in Table 3. At all temperatures, values of  $\Delta G^0$  were negative, indicating that AMX adsorption on both adsorbents was feasible and a spontaneous process. Moreover, a decrease in negative values of  $\Delta G^0$ , as temperature increased, revealed that the adsorption of AMX on ZnO and ZnO-rGO becomes more favourable at higher temperatures. The positive value

**Table 3:** Effect of temperature on AMX adsorption and thermodynamics parameters

Adsorbent	<i>T</i> (K)	q <sub>m</sub> (mq/q)	Therm	odynamics	parameters
		(ilig/g)	∆ <i>G</i> (kJ mol <sup>-1</sup> )	∆ <i>H</i> (kJ mol <sup>-1</sup> )	$\Delta S$ (J mol <sup>-1</sup> K <sup>-1</sup> )
ZnO	308	21.75	-8.98		
	318	22.25	-9.78	19.67	92.86
	328	22.75	-10.69		
	338	23.25	-11.79		
ZnO-rGO	308	225	-15.6		
	318	232.5	-17.18	46.77	201.66
	328	237.5	-18.69		
	338	245	-21.92		

of enthalpy also implied that the process was endothermic. Furthermore, the positive value of  $\Delta S^0$  implies that randomness was increasing throughout the adsorption process [46].

## 3.8 Degradation mechanism of AMX

The degradation experiment was carried out at room temperature (35°C). When AMX solution and catalyst (ZnOrGO) were subjected to diffuse light, a hole ( $h^+$ ) was created in VB of ZnO. These electrons were received at the surface of rGO, which was a good electron acceptor, and reacted with  $O_2$  available in an aqueous solution, forming superoxide radical ( $O_2^-$ ). On the other hand, hole ( $h^+$ ) generated in VB captured  $H_2O$  or  $OH^-$  ions and produced 'OH radicals,

which acted as oxidizing agents, converting AMX into degraded products. The degradation mechanism relies on the electron–hole pair recombination rate. The recombination rate was quite fast in pure ZnO, which eventually delayed the degradation rate. However, in ZnO-rGO, excited electrons were received at the surface of rGO, which increased the time duration of the electron pair recombination period and accelerated the degradation process. First, AMX gets adsorbed on the adsorbent material by  $\pi$ – $\pi$  interaction between aromatic rings of rGO and AMX, and then its degradation takes place. The mechanism of AMX degradation is presented in the following steps [35]:

$$ZnO + light \rightarrow ZnO(h^+ + e^-),$$
 (9)

$$ZnO(e^{-}) + rGO \rightarrow ZnO + RGO(e^{-}),$$
 (10)

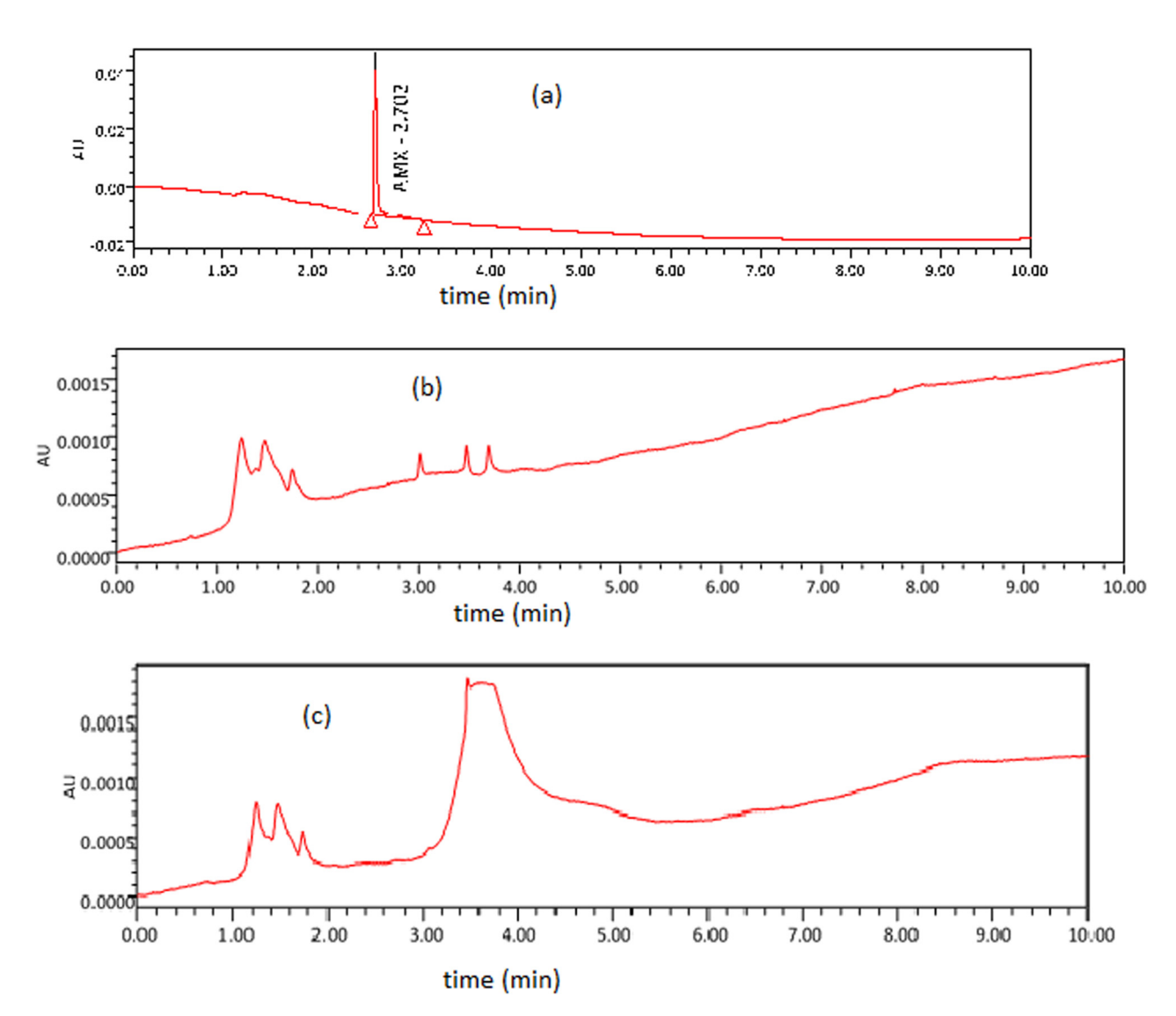


**Figure 7:** (a) HPLC chromatogram of AMX, (b) HPLC chromatogram of AMX degraded products after reaction with ZnO-rGO, and (c) HPLC chromatogram of AMX degraded products after reaction with ZnO.

12 — Mehwish Amanat *et al.* DE GRUYTER

Adsorbent material	Synthesis method	Light source	Concentration of AMX (mg/L)	Adsorbent dosage (mg)	Contact time (min)	Removal efficiency (%)	References
ZnO NPs		UV light	15	2 g/L	15	48.6	[48]
Zno NPs	Precipitation method	Ultrasound	6.25	0.1 g	09	66	[49]
Zno NPs		UV light	104	0.5 g/L	180	100	[20]
ZnO NPs		Ultrasonic waves	150	0.05 g/L	09	92.47	[51]
ZnO-TiO <sub>2</sub> nanocomposite	Ball milling	visible light	100	0.1 g/L	70	80	[4]
GO/TiO <sub>2</sub>		UV light	50	0.4 g/L	09	99.84	[46]
NiO	Sol-gel process	UV light	25	0.2 g/L	120	96	[45]
TiO <sub>2</sub>		UV light	30	450 mg/L	270	80	[52]
Iron oxide nanoparticles	Green synthesis ( <i>Ceratonia</i>	Closed system	5	0.04 g/L	200	66	[38]
(gINPs)	siliqua)						
Mn-doped Cu <sub>2</sub> O NPs	Green synthesis (Aloe vera)	Sunlight	15	1 g/L	180	92	[38]
Ag/ZnO NPs		UV light	5	0.15 g/L	120	93.7	[23]
ZnO NPs	Green Synthesis ( <i>L. chinensis</i> )		5	5 mg	09	85	Present work
ZnO-rGO NCs	Green Synthesis (L. chinensis)		5	0.5 mg	09	96	Present work

Table 4: Comparison of AMX degradation efficiency of catalysts with other adsorbing material

$$O_2 + rGO(e^-) \rightarrow O_2^{\bullet -} + rGO,$$
 (11)

$$H_2O/OH^- + h^+ \to OH,$$
 (12)

•OH/
$$O_2$$
• + AMX  $\rightarrow$  degraded products. (13)

## 3.9 HPLC analysis

The degradation of AMX was confirmed by HPLC analysis. A well-defined chromatogram of standard AMX, as shown in Figure 7(a), is obtained at a retention time of 2.70 min with a 1 mL/min flow rate of mobile phase (methanol:DI water) at 228 nm wavelength. No peak was observed at a retention time of 2.70 min in chromatograms of AMX degraded by ZnO-rGO and ZnO in Figure 7(b) and (c), which confirmed the degradation of AMX into its by-products. The degraded products reported in the literature are AMX penicilloic acid, AMX penicilloic acid, AMX diketopiperazine, and phenol hydroxypyrazine [47].

## 3.10 Comparison with literature

AMX degradation efficiency of ZnO and ZnO-rGO has been compared with other adsorbing materials, as shown in Table 4.

## 3.11 Recyclability of catalysts

Recyclability is a crucial feature of heterogeneous catalysts for their practical applications. The reusability of ZnO NPs

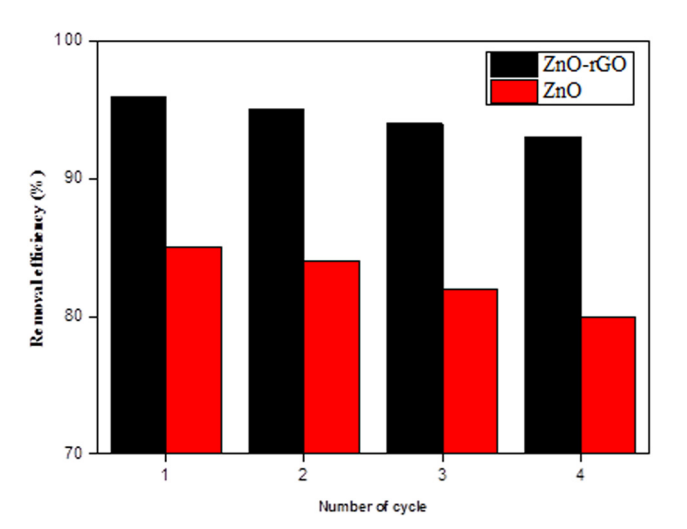


Figure 8: Recyclability of catalysts.

and ZnO-rGO was investigated under optimum conditions for four consecutive cycles. The catalysts were collected after each run from the reaction mixture by centrifugation, washed with distilled water, and dried in an oven at 60°C. It was found that the degradation of AMX by ZnO-rGO is slightly reduced from 96 to 93% after four cycles, while in the case of ZnO NPs, AMX degradation decreased from 85 to 80%, as shown in Figure 8. Figure 8 shows the recyclability of ZnO NPs and ZnO-rGO for the degradation of AMX. A small loss in the catalytic efficiency confirmed that both catalysts have good stability [49].

## 4 Conclusion

ZnO NPs and ZnO-rGO NCs were prepared using the leaf extract of the L. chinensis plant and applied in AMX degradation. The spherical and hexagonal morphologies of prepared nanomaterials were confirmed by SEM analysis. The particle sizes of ZnO and ZnO-rGO were 23.4 and 18.7 nm, respectively, as calculated by XRD measurement. The influence of parameters such as the dose of catalyst, AMX concentration, pH, and temperature on the degradation of AMX was also examined. AMX showed maximum degradation under optimum conditions, i.e., 5 mg/L of solution concentration, 65°C temperature, adsorbent dosages of 5 mg (ZnO) and 0.5 mg (ZnO-rGO), and pH values of 8 (ZnO) and 10 (ZnO-rGO). The catalytic activity of ZnO-rGO NCs showed higher potentiality towards AMX degradation (96%) as compared to ZnO NPs (85%). The antioxidant potential of synthesised nanomaterials was also evaluated, and the result showed that NCs exhibited a higher antioxidant potential than ZnO NPs. The isotherm and thermodynamics analysis revealed that AMX adsorption followed the Freundlich model more closely. Also, it was an endothermic and spontaneous process. So, this research demonstrated that the prepared NC was potent, highly efficient, and suitable adsorbents for the removal and degradation of AMX. It was also confirmed by HPLC.

Funding information: S. J. Park was supported by the Basic Research Program through the National Research Foundation of Korea (NRF) funded by the Ministry of Education (No. 2018R1A6A1A03025526 and No. 2020R1I1A3063782). This work was also supported by the BK-21 FOUR program through the National Research Foundation of Korea (NRF) under the Ministry of Education. The authors thank the Cooperative Equipment Center at KOREATECH for assistance with SEM analysis. This work was funded by the Researchers Supporting Project Number (Project No. RSPD2023R672), King Saud University, Riyadh, Saudi Arabia.

Author contribution: M.A.: writing original manuscript; T.S., S.J.P.: supervision; T.R.: validation; M.Z.: data curation, methodology; F.N.: resources; A.M.T.: software; M.R.K., D.W.: revising manuscript. All authors have accepted responsibility for the entire content of this manuscript and approved its submission.

**Conflict of interest:** The authors state no conflict of interest.

Data availability statement: All data generated or analysed during this study are included in this published article.

## References

- Sharma M, Rajput D, Kumar V, Jatain I, Aminabhavi TM, Mohanakrishna G, et al. Photocatalytic degradation of four emerging antibiotic contaminants and toxicity assessment in wastewater: A comprehensive study. Environ Res. 2023;231:116132. doi: 10.1016/j.envres.2023.116132.
- Nassri I, Souabi S. Occurrence, pollution sources, and mitigation [2] prospects of Antibiotics, anti-inflammatories, and endocrine disruptors in the aquatic environment. Environ Nanotechnol Monit Manag. 2023;20:100878. doi: 10.1016/j.enmm.2023.100878.
- Jian Z, Zeng L, Xu T, Sun S, Yan S, Yang L, et al. Antibiotic resistance [3] genes in bacteria: Occurrence, spread, and control. J Basic Microbiol. 2021;61(12):1049-70. doi: 10.1002/jobm.202100201.
- ۲**4**٦ Thi TDN, Nguyen LH, Nguyen XH, Phung HV, Vinh THT, Van Viet P, et al. Enhanced heterogeneous photocatalytic perozone degradation of amoxicillin by ZnO modified TiO2 nanocomposites under visible light irradiation. Mater Sci Semicond Proc. 2022;142:106456. doi: 10.1016/j.mssp.2022.106456.
- [5] Cetecioglu Z, Atasoy M. Biodegradation and inhibitory effects of antibiotics on biological wastewater treatment systems. Toxicity and Biodegradation Testing. New York, NY: Humana Press; 2018. p. 29-55.
- Tang X, Fan W, Zhang S, Yan B, Zheng H. The improvement of levofloxacin and tetracycline removal from simulated water by thermosensitive flocculant: Mechanisms and simulation. Sep Purif Technol. 2023;309:123027. doi: 10.1016/j.seppur.2022.123027.
- Guo Y. Removal ability of antibiotic resistant bacteria (Arb) and antibiotic resistance genes (Args) by membrane filtration process. IOP Conference Series: Earth Environ Sci. Vol. 801. IOP Publishing; 2021. p. 012004. doi: 10.1088/1755-1315/801/1/012004.
- Subaihi A, Shahat A. Synthesis and characterization of super high [8] surface area silica-based nanoparticles for adsorption and removal of toxic pharmaceuticals from aqueous solution. Jo Mol Liq. 2023;378:121615. doi: 10.1016/j.molliq.2023.121615.
- Zhang D, Liu Y, Song Y, Sun X, Liu W, Duan J, et al. Synergistic effect of Fe and Ce on Fe doped CeO2 for catalytic ozonation of amoxicillin: Efficiency evaluation and mechanism study. Sep Purif Technol. 2023;31:123430. doi: 10.1016/j.seppur.2023.123430.
- Al-Musawi TJ, Yilmaz M, Ramírez-Coronel AA, Al-Awsi GRL, Alwaily ER, Asghari A, et al. Degradation of amoxicillin under a UV or visible light photocatalytic treatment process using Fe2O3/ bentonite/TiO2: Performance, kinetic, degradation pathway,

- energy consumption, and toxicology studies. Optik. 2023;272:170230. doi: 10.1016/j.ijleo.2022.170230.
- [11] Laksaci H, Belhamdi B, Khelifi O, Khelifi A, Trari M. Elimination of amoxicillin by adsorption on coffee waste based activated carbon. J Mol Struct. 2023;274:134500. doi: 10.1016/j.molstruc.2022.134500.
- [12] Lonkar SP, Pillai V, Abdala A. Solvent-free synthesis of ZnO-graphene nanocomposite with superior photocatalytic activity. Appl Surf Sci. 2019;465:1107–13. doi: 10.1016/j.apsusc.2018.09.264.
- [13] Yaqoob AA, Mohd Noor NHB, Serrà A, Mohamad Ibrahim MN. Advances and challenges in developing efficient graphene oxide-based ZnO photocatalysts for dye photo-oxidation. Nanomater. 2020;10:932. doi: 10.3390/nano10050932.
- [14] Zhou Y, Cao S, Xi C, Li X, Zhang L, Wang G, et al. A novel Fe3O4/ graphene oxide/citrus peel-derived bio-char based nanocomposite with enhanced adsorption affinity and sensitivity of ciprofloxacin and sparfloxacin. Bioresour Technol. 2019;292:121951. doi: 10.1016/ j.biortech.2019.121951.
- [15] Ramesh AM, Pal K, Kodandaram A, Manjula BL, Ravishankar DK, Gowtham HG, et al. Antioxidant and photocatalytic properties of zinc oxide nanoparticles phyto-fabricated using the aqueous leaf extract of Sida acuta. Green Proc Synth. 2022;11(1):857–67. doi: 10.1515/gps-2022-0075.
- [16] Hamed R, Obeid RZ, Abu-Huwaij R. Plant mediated-green synthesis of zinc oxide nanoparticles: An insight into biomedical applications. Nanotechnol Rev. 2023;12(1):20230112. doi: 10.1515/ntrev-2023-0112.
- [17] Sadhukhan S, Bhattacharyya A, Rana D, Ghosh TK, Orasugh JT, Khatua S, et al. Synthesis of RGO/NiO nanocomposites adopting a green approach and its photocatalytic and antibacterial properties. Mater Chem Phys. 2020;247:122906. doi: 10.1016/j.matchemphys. 2020.122906.
- [18] Rad SS, Sani AM, Mohseni S. Biosynthesis, characterization and antimicrobial activities of zinc oxide nanoparticles from leaf extract of *Mentha pulegium* (L.). Microb Pathog. 2019;131:239–45. doi: 10.1016/j.micpath.2019.04.022.
- [19] Kanwal A, Shahzadi T, Riaz T, Zaib M, Khan S, Habila MA, et al. Photocatalytic degradation studies of organic dyes over novel Cu/ Ni loaded reduced graphene oxide hybrid nanocomposite: adsorption, kinetics and thermodynamic studies. Mol. 2023;28(18):6474. doi: 10.3390/molecules28186474.
- [20] Lee KG, Shibamoto T. Antioxidant property of aroma extract isolated from clove buds *Syzygium aromaticum* (L.) [Merr. et Perry]. Food Chem. 2001;74:443–8. doi: 10.1016/s0308-8146(01)00161-3.
- [21] Makkar HPS, Blümmel M, Borowy NK, Becker K. Gravimetric determination of tannins and their correlations with chemical and protein precipitation methods. J Sci Food Agric. 1993;61:161–5. doi: 10.1002/jsfa.2740610205.
- [22] Prieto P, Pineda M, Aguilar M. Spectrophotometric quantitation of antioxidant capacity through the formation of a phosphomolybdenum complex: specific application to the determination of vitamin E. Anal Biochem. 1999;269:337–41. doi: 10.1006/abio.1999.4019.
- [23] Balarak D, Mahvi AH, Shim MJ, Lee SM. Adsorption of ciprofloxacin from aqueous solution onto synthesized NiO: isotherm, kinetic and thermodynamic studies. Desalin Water Treat. 2021;212:390–400. doi: 10.5004/dwt.2021.26603.
- [24] Shahzadi T, Anwaar A, Riaz T, Zaib M. Sulfate and phosphate ions removal using novel nano-adsorbents: modeling and optimization, kinetics, isotherm and thermodynamic studies. Int J Phytoremediat. 2022;24:1518–32. doi: 10.1080/15226514.2022.2040421.
- [25] Kaur R, Avti P, Kumar V, Kumar R. Effect of various synthesis parameters on the stability of size controlled green synthesis of

- silver nanoparticles. Nano Express. 2021;2:020005. doi: 10.1088/2632-959x/abf42a.
- [26] Agarwal V, Zetterlund PB. Strategies for reduction of graphene oxide–A comprehensive review. Chem Eng J. 2021;405:127018. doi: 10.1016/j.cej.2020.127018.
- [27] Ahmadi R, Nafchi RF, Sangpour P, Bagheri M, Badiei E. A comparative study: Green synthesis and evaluation of ZnO-GO and ZnO-RGO nanocomposites for antibacterial applications. Mater Sci Eng. 2023;294:116555. doi: 10.2139/ssrn.4270332.
- [28] Kumar S, Ojha AK, Walkenfort B. Cadmium oxide nanoparticles grown in situ on reduced graphene oxide for enhanced photocatalytic degradation of methylene blue dye under ultraviolet irradiation. J Photochem Photobiol B: Biol. 2016;159:111–9. doi: 10.1016/i.jphotobiol.2016.03.025.
- [29] Sai Saraswathi V, Tatsugi J, Shin PK, Santhakumar K. Facile biosynthesis, characterization, and solar assisted photocatalytic effect of ZnO nanoparticles mediated by leaves of L. speciosa. J Photochem Photobiol B: Biol. 2017;167:89–98. doi: 10.1016/j. jphotobiol.2016.12.032.
- [30] Murali A, Sarswat PK, Free ML. Minimizing electron-hole pair recombination through band-gap engineering in novel ZnO-CeO2rGO ternary nanocomposite for photoelectrochemical and photocatalytic applications. Env Sci Pollut Res. 2020;27:25042–56. doi: 10. 1007/s11356-020-08990-z.
- [31] Hidayah NMS, Liu WW, Lai CW, Noriman NZ, Khe CS, Hashim U et al. Comparison on graphite, graphene oxide and reduced graphene oxide: Synthesis and characterization. AIP Conference Proceedings. AIP Publishing LLC; 2017. p. 150002.
- [32] Boukhvalov DW, Katsnelson MI. Tuning the gap in bilayer graphene using chemical functionalization: Density functional calculations. Phys Rev B. 2008;78(8):085413. doi: 10.1103/physrevb.78.085413.
- [33] Rajiv P, Rajeshwari S, Venckates R. Bio-Fabrication of zinc oxide nanoparticles using leaf extract of Parthenium hysterophorus L. and its size-dependent antifungal activity against plant fungal pathogens. Spectrochim Acta Mol Biomol Spectrosc. 2013;112:384–7. doi: 10.1016/j.saa.2013.04.072.
- [34] Jain B, Hashmi A, Sanwaria S, Singh AK, Susan MABH, Singh A. Zinc oxide nanoparticle incorporated on graphene oxide: an efficient and stable photocatalyst for water treatment through the Fenton process. Adv Compos Hybrid Mater. 2020;3:231–42. doi: 10.1007/s42114-020-00153-5.
- [35] Gang R, Xu L, Xia Y, Zhang L, Wang S, Li R. Facile one-step production of 2D/2D ZnO/rGO nanocomposites under microwave irradiation for photocatalytic removal of tetracycline. ACS Omega. 2021;6(5):3831–9. doi: 10.1021/acsomega.0c05559.
- [36] Wu S, Zhao X, Li Y, Du Q, Sun J, Wang Y, et al. Adsorption properties of doxorubicin hydrochloride onto graphene oxide: equilibrium, kinetic and thermodynamic studies. Mater. 2013;6:2026–42. doi: 10.3390/ma6052026.
- [37] Zhao D, Sheng G, Chen C, Wang X. Enhanced photocatalytic degradation of methylene blue under visible irradiation on graphene@TiO<sub>2</sub> dyade structure. Appl Catal B: Environ. 2012;111–112:303–8. doi: 10.1016/j.apcatb.2011.10.012.
- [38] Gaim YT, Yimanuh SM, Kidanu ZG. Enhanced photocatalytic degradation of amoxicillin with MN-doped cu<sub>2</sub>o under sunlight irradiation. J Compos Sci. 2022;6(10):317. doi: 10.3390/jcs6100317.
- [39] Aksu Demirezen D, Yıldız YE, Demirezen Yılmaz D. Amoxicillin degradation using green synthesized iron oxide nanoparticles: Kinetics and mechanism analysis. Env Nanotechnol Monit Manag. 2019;11:100219. doi: 10.1016/j.enmm.2019.100219.

- [40] Rodrigues DLC, Machado FM, Osório AG, de Azevedo CF, Lima EC, da Silva RS, et al. Adsorption of amoxicillin onto high surface area-activated carbons based on olive biomass: kinetic and equilibrium studies. Env Sci Pollut Res. 2020;27:41394–404. doi: 10.1007/ s11356-020-09583-6.
- [41] Shahzadi T, Rehman S, Riaz T, Zaib M. Eco-friendly synthesis of ZnO nanoparticles using Cannabis sativa and assessment of its activities as efficient dyes removal and antioxidant agent. Int J Env Anal Chem. 2022;102(16):4738–56. doi: 10.1080/03067319.2020.1789610.
- [42] Masfria S, Dalimunthe Rasayan A. Determination of total phenolic content, total flavonoid content, and antimutagenic activity of ethanol extract nanoparticles of *Rhaphidophora Pinnata* (L.F) *Schott* leaves. Rasayan J Chem. 2018;11:505–10. doi: 10.31788/rjc.2018. 1122068.
- [43] Balarak D, Mostafapour FK, Joghtaei A. Thermodynamic analysis for adsorption of amoxicillin onto magnetic carbon nanotubes. Br J Pharma Res. 2017;16:1–11. doi: 10.9734/bjpr/2017/33212.
- [44] Duman O, Ayranci E. Adsorption characteristics of benzaldehyde, sulphanilic acid, and p-phenolsulfonate from water, acid, or base solutions onto activated carbon cloth. Sep Sci Technol. 2006;41:3673–92. doi: 10.1080/01496390600915072.
- [45] Balarak D, Mostafapour FK. Photocatalytic degradation of amoxicillin using UV/synthesized NiO from pharmaceutical wastewater. Indones J Chem. 2019;19:211. doi: 10.22146/ijc.33837.
- [46] Balarak D, Mengelizadeh N, Rajiv P, Chandrika K. Photocatalytic degradation of amoxicillin from aqueous solutions by titanium dioxide nanoparticles loaded on graphene oxide. Env Sci Pollut Res. 2021;28(36):49743–54. doi: 10.1007/s11356-021-13525-1.

- [47] Gozlan I, Rotstein A, Avisar D. Amoxicillin-degradation products formed under controlled environmental conditions: Identification and determination in the aquatic environment. Chemosphere. 2013;91:985–92. doi: 10.1016/j.chemosphere.2013.01.095.
- [48] Fazilati M, Hassani A, Torabian A. Photocatalytic degradation of amoxicillin and cephalexin from aqueous solution by Zno And Tio<sub>2</sub>. In International Congress on Engineering Science and Sustainable Urban Development Denmark; 2018. p. 1–10.
- [49] Ayanda OS, Aremu OH, Akintayo CO, Sodeinde KO, Igboama WN, Oseghe EO, et al. Sonocatalytic degradation of amoxicillin from aquaculture effluent by zinc oxide nanoparticles. Env Nanotechnol Monit Manag. 2021;16:100513. doi: 10.1016/j.enmm.2021.100513.
- [50] Elmolla ES, Chaudhuri M. Degradation of amoxicillin, ampicillin and cloxacillin antibiotics in aqueous solution by the UV/ZnO photocatalytic process. J Hazard Mater. 2010;173(1–3):445–9. doi: 10.1016/j. jhazmat.2009.08.104.
- [51] Rahdar S, Ahmadi S. The removal of amoxicillin with Zno nanoparticles in combination with US-H<sub>2</sub>O<sub>2</sub> advanced oxidation processes from aqueous solutions. Iran J Health Sci. 2019;7(1):36–45. doi: 10.18502/jhs.v7i1.1023.
- [52] Verma M, Haritash A. Photocatalytic degradation of amoxicillin in pharmaceutical wastewater: A potential tool to manage residual antibiotics. Env Technol Innov. 2020;20:101072. doi: 10.1016/j.eti. 2020.101072.
- [53] Rezaei MR, Sayadi MH, Ravankhah N. Photocatalytic degradation of amoxicillin and levofloxacin from aqueous solutions using Ag/ZnO. J Nat Environ. 2021;74(2):331–44. doi: 10.22059/JNE.2021. 318062.2160.